Materials Today Bio 23 (2023) 100811

Contents lists available at ScienceDirect

Materials Today Bio

journal homepage: www.journals.elsevier.com/materials-today-bio

Melatonin-loaded self-healing hydrogel targets mitochondrial energy metabolism and promotes annulus fibrosus regeneration

Xiayu Hu [a,b,1], Xin Tian [a,b,1], Chunju Yang [a,b,c,1], Feng Ling [a,b,d], Hao Liu [a], Xuesong Zhu [a,b], Ming Pei [e], Huilin Yang [a,b], Tao Liu [a,*], Yong Xu [a,b,**], Fan He [a,b,***]

[a] Department of Orthopaedics, The First Affiliated Hospital of Soochow University, Soochow University, Suzhou 215006, China
[b] Orthopaedic Institute, Suzhou Medical College, Soochow University, Suzhou 215000, China
[c] Suzhou Medical College of Soochow University, Suzhou, 215123, China
[d] Department of Orthopaedics,the Affiliated Taizhou People's Hospital of Nanjing Medical University, Taizhou, 225300, China
[e] Stem Cell and Tissue Engineering Laboratory, Department of Orthopaedics and Division of Exercise Physiology, West Virginia University, Morgantown, WV 26506, USA

ARTICLE INFO

Keywords:
Annulus fibrosus
Melatonin
Mitochondrial function
Self-healing hydrogel
NRF2

ABSTRACT

Intervertebral disc (IVD) herniation is a major cause of chronic low back pain and disability. The current nucleus pulposus (NP) discectomy effectively relieves pain symptoms, but the annulus fibrosus (AF) defects are left unrepaired. Tissue engineering approaches show promise in treating AF injury and IVD degeneration; however, the presence of an inflammatory milieu at the injury site hinders the mitochondrial energy metabolism of AF cells, resulting in a lack of AF regeneration. In this study, we fabricated a dynamic self-healing hydrogel loaded with melatonin (an endocrine hormone well-known for its antioxidant and anti-inflammatory properties) and investigate whether melatonin-loaded hydrogel could promote AF defect repair by rescuing the matrix synthesis and energy metabolism of AF cells. The protective effects of melatonin on matrix components (e.g. type I and II collagen and aggrecan) in AF cells were observed in the presence of interleukin (IL)-1β. Additionally, melatonin was found to activate the nuclear factor erythroid 2-related factor signaling pathway, thereby safeguarding the mitochondrial function of AF cells from IL-1β, as evidenced by the increased level of adenosine triphosphate, mitochondrial membrane potential, and respiratory chain factor expression. The incorporation of melatonin into a self-healing hydrogel based on thiolated gelatin and β-cyclodextrin was proposed as a means of promoting AF regeneration. The successful implantation of melatonin-loaded hydrogel has been shown to facilitate *in situ* regeneration of AF tissue, thereby impeding IVD degeneration by preserving the hydration of nucleus pulposus in a rat box-cut IVD defect model. These findings offer compelling evidence that the development of a melatonin-loaded dynamic self-healing hydrogel can promote the mitochondrial functions of AF cells and represents a promising strategy for IVD regeneration.

1. Introduction

Chronic low back pain (LBP) is the leading cause of disability worldwide, affecting patients' quality of life and imposing a massive burden on public health [1]. Intervertebral disc (IVD) degeneration is the leading cause of LBP, primarily due to aging, mechanical overloading, or the following injury [2]. The native IVD is the largest avascular structure in the body, consisting of the inner gel-like nucleus pulposus (NP), the outer fibrocartilaginous annulus fibrosis (AF), and the upper and lower cartilage endplates (EP). The AF is organized into a lamellar architecture as an important component of the IVD to withstand spine loading and resist shear stress during body motion. Oriented type I collagen (COL I) fibrils that provide anti-tension support mainly distribute on the outside layer in the extracellular matrix (ECM) of AF, while non-oriented type II collagen (COL II) fibrils and negatively charged proteoglycans that resist axial compression are present in the

* Corresponding author. Department of Orthopaedics, The First Affiliated Hospital of Soochow University, No. 899 Pinghai Road, Suzhou 215006, Jiangsu, China.
** Corresponding author. Orthopaedic Institute, Medical College, Soochow University, No. 178 East Ganjiang Road, Suzhou 215000, Jiangsu, China
*** Corresponding author. Orthopaedic Institute, Medical College, Soochow University, No. 178 East Ganjiang Road, Suzhou 215000, Jiangsu, China
E-mail addresses: liutao8250@suda.edu.cn (T. Liu), yxu1615@suda.edu.cn (Y. Xu), fanhe@suda.edu.cn (F. He).
[1] Xiayu Hu, Xin Tian, and Chunju Yang contributed equally to this work.

https://doi.org/10.1016/j.mtbio.2023.100811
Received 8 June 2023; Received in revised form 21 August 2023; Accepted 21 September 2023
Available online 22 September 2023

inner side close to the NP [3]. Damage to the AF during IVD degeneration may result in abnormal mechanical stress, loss of physiological functions, and IVD herniation, where dehydrated NP tissue can protrude through AF defects, compressing the nerve root and spinal cord and causing neuropathy [4].

Oxidative stress, referring to the imbalance between generating and scavenging reactive oxygen species (ROS), has played a critical role in IVD degeneration [5]. ROS include superoxide anion, oxygen singlet, hydroxyl radical, and hydrogen peroxide (H_2O_2). The highly active ROS damages the nucleic acid, proteins, and lipids and induces IVD cell apoptosis to accelerate the degeneration [6]. When AF cells are exposed to advanced glycation end-products (AGEs), it results in cell death by increasing cytochrome *c* release from mitochondria into the cytosol and subsequently activating the caspase 3-mediated apoptotic signaling cascade [7]. Regarding IVD matrix metabolism, Dimozi et al. treated human IVD cells with H_2O_2 at sublethal concentrations. They discovered ECM synthesis was inhibited in H_2O_2-treated cells with up-regulation of ECM-degrading proteases, such as matrix metalloproteinase-1, -2, and -9 [8]. Although the electron transport chain generates most ROS, mitochondria are the primary target of ROS attack, and mitochondrial dysfunction is closely related to IVD degeneration. ROS over-accumulation induces damage to mitochondrial DNA and respiratory enzymes, resulting in mitochondrial dysfunction, such as mitochondrial membrane depolarization, compromised membrane integrity, decreased adenosine triphosphate (ATP) production, and dysregulation of mitochondrial fusion and fission [9]. Abnormal mitochondria morphology has been observed in degenerated IVD cells. In a previous study, Hartman et al. identified age-related bioenergetic changes in IVD cells derived from rabbits, and they demonstrated that aging reduced mitochondrial number and glycolytic capacity and suppressed matrix synthesis [10]. Therefore, restoring the mitochondrial function impaired by oxidative stress in IVD cells may be a promising strategy for treating IVD degeneration.

Melatonin (N-acetyl-5-methoxytraptamine), primarily produced in the pineal gland, is well-known for its antioxidant property to scavenge free radicals. Additionally, melatonin attenuates oxidative stress by stimulating intracellular antioxidant enzymes, such as catalase (CAT), superoxide dismutase (SOD), heme oxygenase (HO-1), and glutathione peroxidase (GPX) [11]. Melatonin-mediated protection against oxidative stress involves the nuclear factor erythroid 2-related factor (NRF2) signaling pathway. When ROS stimulates, NRF2 is translocated into the nucleus and binds to antioxidant response elements (ARE) to promote the transcription of antioxidant and detoxification genes [12]. Recently, melatonin has effectively ameliorated IVD degeneration by protecting NP cells from oxidative stress-induced apoptosis [13], regulating NP ECM remodeling induced by interleukin (IL)-1β [14], and preventing cartilage endplate chondrocyte calcification [15]. Chen et al. revealed that the protective effect of melatonin on NP cells depended on mitophagy stimulation, a self-protective mechanism to maintain mitochondrial function, via activation of the upstream regulator Parkin, indicating the involvement of mitochondrial homeostasis in melatonin-mediated protection on IVD [16]. A recent study from our laboratory illustrates that melatonin recharged the impaired mitochondria to rescue energy metabolism and matrix synthesis capacity of articular chondrocytes derived from rat cartilage suffering from post-traumatic osteoarthritis (OA), an age-related disease with similar pathological processes with IVD degeneration [17]. Therefore, considering the importance of AF in maintaining IVD biomechanical functions, it is worth investigating the effect of melatonin on repairing AF defects in degenerative IVD.

The ability of damaged IVD to self-repair is limited due to a lack of blood vessels. Injectable hydrogel, as a minimally invasive approach, represents a new strategy for restoring or regenerating the structure and biological function of IVD. Hydrogel consists of three-dimensional cross-linked networks formed by hydrophilic polymers. They have attracted great attention due to their high biocompatibility, controllable degradation rate, and nontoxic degradation products in IVD tissue engineering [18]. An interpenetrating hydrogel network with strength and toughness properties supports long-term cell survival and facilitates NP regeneration in rat degenerative IVDs [19]. Regarding AF regeneration, DiStefano et al. developed an injectable hydrogel composed of poly (ethylene glycol) diacrylate (PEGDA) and fibrin to strengthen adhesion to the AF tissue surface. This hydrogel successfully repaired AF defects as a surgical sealant in an *ex vivo* bovine model of discectomy [20]. Additionally, the self-healing ability is an important property of hydrogel used in AF regeneration since it can provide stronger mechanical performance and a longer endurance life during the dynamic healing of the damaged AF tissue [21].

Self-healing materials belong to the category of intelligent materials capable of autonomously repairing damage without the need for external intervention [22]. The structural integrity of the hydrogel network can be compromised by mechanical forces resulting from routine bodily movements, thereby diminishing the therapeutic efficacy of the hydrogel [23]. Nevertheless, self-healing hydrogels exhibit superior mechanical support and the ability to restore their initial structure without compromising functionality, owing to their reversible dynamic linkage within the network, in contrast to conventional hydrogels when the network is disrupted [24]. The primary challenge in the healing of AF lies in ensuring that it acquires mechanical properties comparable to those of the native tissue, while also preserving its structural integrity [25], This challenge can be effectively addressed through the utilization of self-healing hydrogels. Our laboratory previously fabricated a self-healing hydrogel based on mercapto-modified gelatin and gold ions, and it can create a supramolecular envelope with kartogenin via a cyclodextrin-mediated host-guest reaction [26]. Nevertheless, few dynamic hydrogels exhibit bioactivity on AF matrix metabolism or influence mitochondrial redox homeostasis. Thus, incorporating melatonin into self-healing hydrogel is necessary to improve hydrogel's biological performance.

Based on these observations, we hypothesized that melatonin could enhance AF matrix anabolism by preserving the mitochondrial energy metabolism in an IL-1β-induced inflammatory environment. Mechanistically, we investigated the effect of melatonin on mitochondrial redox homeostasis of AF cells via activating the NRF2-mediated antioxidant pathway. Finally, we developed a self-healing hydrogel incorporating melatonin (hydrogel@MT) and evaluated the therapeutic potential of this composite in repairing AF defects in a rat caudal IVD model (Fig. 1).

2. Methods and materials

2.1. Isolation and culture of AF cells

AF tissues were harvested from four Sprague-Dawley (SD) rats (eight-week-old, male). After removing the ligaments, muscles, and NP tissues, the rat caudal AF tissues were collected under aseptic conditions and digested in 2 mg/mL of type I and II collagenase solution (Thermo Fisher Scientific, Waltham, MA, USA) at 37 °C for 5 h. The suspension was centrifuged at 1200 rpm for 5 min after filtering through a 100-μm strainer (Thermo Fisher Scientific). Primary AF cells were re-suspended and cultured in F12 Dulbecco's Modified Eagle Medium (DMEM/F12) supplemented with 10% fetal bovine serum (FBS), 100 U/mL penicillin, and 100 μg/mL streptomycin (all from Thermo Fisher Scientific) in a humidified incubator at 37 °C with 5% CO_2. AF cells of Passage Two were used for the subsequent experiments.

2.2. In vitro treatments

Melatonin (MT; Sigma-Aldrich, St. Louis, MO, USA) was dissolved in dimethyl sulfoxide (DMSO; Sigma-Aldrich) to create a stock solution of 250 mM and then diluted to different concentrations in DMEM/F12. AF cells were treated with 5 ng/mL recombinant human IL-1β (Thermo Fisher Scientific) to induce an inflammatory environment. Then, the

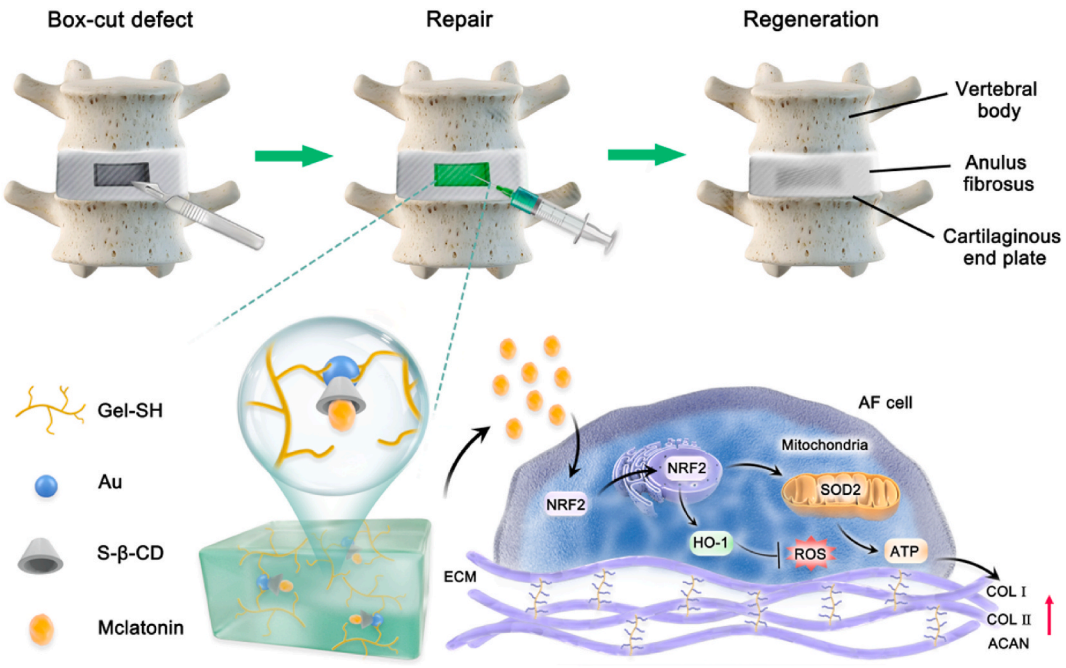

Fig. 1. The present study depicts a schematic diagram of a self-healing hydrogel loaded with melatonin, which facilitates the regeneration of annulus fibrosus.

cells were treated with 1 and 100 μM MT, while the control group was exposed to an equal volume of DMSO (0.4 μL DMSO/mL medium).

2.3. Reverse transcription-quantitative polymerase chain reaction (RT-qPCR)

The total RNA was extracted from AF cells using TRIzol Reagent (Vazyme, Nanjing, China), and its concentration was measured using a NanoDrop 2000 spectrophotometer (Thermo Fisher Scientific). Complementary DNA (cDNA) was generated from 1 μg of RNA via the first-strand cDNA synthesis reaction using an ABScriptIII reverse transcriptase kit (ABclonal Technology, Wuhan, China). The primer sequences are listed in Supplementary Table 1. RT-qPCR was performed with SYBRGreen Master Mix (ABclonal Technology) using a CFX96 qPCR system (Bio-Rad, Hercules, CA, USA). Results were quantified using the $2^{-\triangle\triangle CT}$ method with glyceraldehyde-3-phosphate dehydrogenase (*Gapdh*) as a housekeeping gene.

2.4. Western blot

Total cellular protein was extracted using radioimmunoprecipitation assay (RIPA) lysis buffer (Beyotime Biotech. Inc., Shanghai, China), and the concentration was determined using a bicinchoninic acid (BCA) protein assay kit (Beyotime). The protein was denatured at 100 °C, separated by electrophoresis in a 10% polyacrylamide gel, and then transferred onto a nitrocellulose membrane. The membrane was blocked at room temperature for 30 min and incubated with a properly diluted primary antibody (Abcam, Cambridge, UK) at 4 °C overnight. Then, the membrane was incubated with a goat anti-rabbit IgG (H&L) secondary antibody (Abcam) at room temperature for 1 h. The bands were visualized with a chemiluminescence solution (Vazyme) using Chemical luminescence imaging system (Clinx Science Instruments Co., Ltd, Shanghai, China). The relative protein expression was calculated according to the band intensity using the ImageJ software (National Institutes of Health, Bethesda, MD, USA). The primary antibodies are listed in Supplementary Table 2.

2.5. Immunofluorescence staining

The samples were fixed with 4% paraformaldehyde (Sigma-Aldrich) for 30 min, permeated with 0.1% Triton-X 100 (Beyotime) for 8 min, and blocked with 5% Bovine Serum Albumin Blocking Buffer (Beyotime) for 30 min at room temperature. After overnight incubation with the primary antibody against COL I (1:500, ab34710, Abcam) or NRF2 (1:500, ab137550, Abcam) at 4 °C, the cells were incubated with Cy3 Goat Anti-Rabbit IgG (1:500, AS007, ABclonal, Whhan, Technology) at room temperature for 1 h. The cytoskeleton F-actin was stained using phalloidin-fluorescein isothiocyanate (FITC) isomer (Sigma-Aldrich) for 20 min, and the nuclei were counterstained with 4′,6-diamidino-2-phenylindole (DAPI; Thermo Fisher Scientific). Fluorescence images were captured using a Zeiss Axiovert 40CFL microscope (Zeiss, Oberkochen, Germany).

2.6. Mitochondrial function evaluation

2.6.1. ATP production

AF cells in six-well plates were collected with 200 μL of lysis buffer per well. The suspension was centrifuged at 12,000 rpm for 5 min at 4 °C. The ATP content in the supernatant was measured using an ATP assay kit (Beyotime) following the manufacturer's instructions. After incubating at room temperature in the dark for 30 min, the optical density of each well was detected using a Centro LB 960 (Berthold Technologies, Bad Wildbad, Germany). The protein concentration of each sample was measured using a BCA kit to normalize the ATP production.

2.6.2. Mitochondrial membrane potential (MMP)

After washing the cell with serum-free medium, they were incubated with JC-1 working staining solution (Beyotime) at 37 °C for 30 min. Immunofluorescence images were captured using a fluorescence microscope and analyzed using ImageJ software. JC-1 aggregates (red) indicated healthy polarized.

2.6.3. Measurement of intracellular ROS and mitochondrial superoxide

AF cells were incubated with 10 μM 2′,7′-dichlorofluorescein diacetate (DCFH-DA; Beyotime) at 37 °C for 30 min in the dark to investigate

intracellular ROS accumulation. The cells were washed with serum-free medium to remove the residual DCFH-DA. Fluorescence images were immediately captured at a wavelength (excitation/emission) of 488/525 nm using a Zeiss fluorescence microscope.

AF cells were incubated with a MitoSOX™ Red Mitochondrial Superoxide Indicator (Thermo Fisher Scientific) at 37 °C for 20 min in the dark following the manufacturer's instructions to measure the mitochondrial superoxide production. Fluorescence images were captured using a Zeiss fluorescence microscope and analyzed using ImageJ software.

2.7. Small interfering RNA (siRNA) transfection

siRNA targeting *Nrf2* (siNRF2) was mixed with Lipofectamine™ 3000 (Thermo Fisher Scientific) at room temperature for 20 min to inhibit *Nrf2* expression and transfected into AF cells at 37 °C for 6 h. After washing with phosphate-buffered saline (PBS; Thermo Fisher Scientific), the cells were incubated with a fresh culture medium for mitochondrial function experiments.

2.8. Fabrication and characterization of MT-loaded self-healing hydrogel

2.8.1. Self-healing hydrogel synthesis

1 g of Gelatin (Sigma-Aldrich) was dissolved in 40 mL of PBS (pH = 8.0) and mercaptoized using 32 mg of Traut's Reagent (Aladdin, Shanghai, China) to synthesize thiolated gelatin. This solution was dialyzed using a dialysis bag (MW cutoff = 3000 Da, Sigma Aldrich) for 7 d and then lyophilized for preservation. Subsequently, 200 mg of thiolated gelatin (dissoved in 1.3 mL of PBS) and 50 mg of 6-deoxy-6-mercapto-β-cyclodextrin (S-β-CD, dissoveld in 350 μL of PBS, Macklin, Shanghai, China) was mixed and heated at 37 °C for 1 h. 10 mg of MT (dissolved in 50 μL of DMSO) was thoroughly mixed in 1.65 mL Gel-β-CD solution in a water bath at 37 °C for 1 h for drug loading. Then, 7 mg of chlorate hydrate solution ($HAuCl_4$, dissolved in 300 μL of PBS, J&K Scientific) was added and stirred thoroughly to fabricate MT-loaded Au-Gel-β-CD self-healing hydrogel.

2.8.2. Characterization of hydrogel morphology

The self-healing hydrogel morphology was observed using scanning electron microscopy (SEM; Regulus SU8100, Tokyo, Japan). A small piece of the self-healing hydrogel was taken and sprayed with gold after being freeze-dried. Then, the morphology and structure of the gold-coated samples were observed using an SEM at an acceleration voltage of 2 kV.

2.8.3. Injectable and self-healing properties

The hydrogel in a syringe was injected using a 22 G needle to investigate its injectable performance. The hydrogels in two square molds were stained with different dyes to verify the self-healing performance. Then, hydrogels were cut into different colors and placed in a 37 °C incubator to observe their self-healing performance.

2.8.4. Rheological properties

The rheological properties of the hydrogel were determined using an AR2000Ex rheometer (Waters Corporation, Milford, MA, USA). The shear storage modulus (G′) and shear loss modulus (G″) were obtained at a constant setting of 37 °C and 1 Hz. The G′ and G″ values of the hydrogel were obtained under alternating oscillating strains of 1% and 300% (low strain 1%, 60 s, high strain 300%, 60 s).

2.8.5. Release profile of melatonin

The MT-loaded hydrogel was soaked in PBS in an incubator at 37 °C. The extracts were collected at specific time points and replaced with the same amount of fresh PBS for one month. According to the standard curve of MT, the cumulative release profiles of MT were determined at the absorbance of 280 nm using a UV–vis spectrophotometer (Shimadzu Co., LTD, Shanghai, China).

2.8.6. Measurement of the total mercapto content

The total mercapto content of the sample was determined by an Micro Total Mercapto Assay Kit (Solarbio Technology Co., LTD, Beijing, China) according to the manufacturer's instructions. After incubation for 10 min at room temperature, the absorbance was measured at 412 nm using an UV–vis spectrophotometer (Shimadzu Co., LTD, Shanghai, China).

2.8.7. Determination of the substitution degree

The substitution degree of the Au-Gel-β-CD hydrogel was determined using trinitrobenzenesulfonic acid (TNBS, Acmec Biochemical Technology CO., Ltd, Shanghai, China). Hydrogel was mixed with 0.1% (w/v) TNBS, and after incubation at 50 °C for 60 min in the dark, the absorbance was measured at 335 nm using an UV–vis spectrophotometer.

2.9. Cytocompatibility of MT-loaded self-healing hydrogel

2.9.1. Cell proliferation

The MT-loaded hydrogel was incubated with PBS for 24 h to extract the leach solution. The cell proliferation was detected using a Cell Counting Kit-8 reagent (CCK-8, Beyotime). AF cells were seeded in a 96-well plate and incubated in the culture medium containing the leach solution. CCK-8 solution was added at different time points and incubated at 37 °C for 2 h. The absorbance was measured at 450 nm using a microplate reader (BioTek Instruments Inc., Winooski, VT, USA).

2.9.2. Cell migration assay

A sterile pipette tip was used to make a straight wound in the cell layer with complete confluence to establish a scratch model. AF cells were cultured in the culture medium containing the leach solution and imaged every 6 h. The cell migration ability was measured by calculating the distance between two edges in the wound area over time and analyzed using Image J software.

2.9.3. Live/dead cell staining

AF cells were seeded in a 24-well plate at 37 °C and treated with or without hydrogel leach solution. The cells were stained using the Live/Dead cell staining kit (Beyotime) at room temperature for 30 min to evaluate the cytotoxicity. The cell images were captured using a Zeiss fluorescence microscope. The dead cells were colored red while living cells were colored green.

2.10. In vivo AF regeneration study

2.10.1. Surgical procedures

The animal experiments were approved by the Ethics Committee of Soochow University (SUDA20230402A04). Thirty-two male SD rats with an average body weight of 300 g were purchased from the Experimental Animal Center of Soochow University and randomly divided into four groups: intact IVD (Sham group), a box defect without treatment (Defect group), a box defect treated with hydrogel (Hydrogel group), and a box defect treated with MT-loaded self-healing hydrogel (Hydrogel@MT group).

After anesthesia with 3% sodium pentobarbital (1.5 mL/kg, Yuanye, China), the rats were placed in the prone position, and the surgical site was routinely disinfected and towel spread. A 3 cm long longitudinal incision was made at the midline of the rear side of the tail. The skin, subcutaneous tissue, and fascia were removed to expose the caudal IVD completely, and the ligaments in the tail were released. The segments Co7-8 and Co8-9 were selected to perform annulotomy, which involved cutting a box defect (2.0 mm × 1.0 mm × 0.8 mm) in the AF tissue [27]. Simultaneously, approximately 5 μL of seal-healing hydrogel or MT-loaded hydrogel was injected into the AF defect. The rat tail skin was

cut without annulotomy in the Sham group. Finally, the incision was sutured, and the surgical site was washed with dilute iodophor. All surgery operations were performed by X.H. After the implantation, rats were placed in cages with adequate food and water.

2.10.2. Diagnostic imaging

After anesthesia, X-ray radiographs (250 mA, 50 kV, and 20 ms) of the rat tails were obtained using an X-ray Photography System (RADspeed M, Shimadzu, Japan). All X-ray images were captured in a sagittal position, and the disc height was measured using the Image J software. The disc height was normalized to the average height of adjacent vertebrae to calculate the disc height index (DHI) that referred to the disc height loss [28].

Magnetic resonance imaging (MRI) was performed using a 1.5 T system (GE Healthcare, Chicago, IL, USA) to obtain the T2-weighted images (TR 3500 ms; TE 120 ms; field of view, 200 × 200 mm; slice thickness, 1.4 mm) to evaluate NP water content. The high signal intensity area in the mid-sagittal of the T2 image was defined as the outline of the NP, and the images were measured using the Image J software.

2.10.3. Histological analysis

The rats were sacrificed four to eight weeks after the surgery, and the vertebral tail specimens were harvested. The samples were fixed with 10% formalin for 48 h, decalcified with 10% ethylenediaminetetraacetic acid (EDTA, Thermo Fisher Scientific), dehydrated with graded ethanol solutions, and embedded with paraffin. The paraffin specimens were cut into 6-μm sections using a microtome (Leica Biosystems, Buffalo Grove, IL, USA). The sections were dewaxed with xylenes (Sigma-Aldrich) and rehydrated with graded ethanol solutions. Histological analysis was performed using hematoxylin and eosin staining (H&E) and Safranin O (S.O.)-fast green staining (all from Solaibao Technology Co., Ltd, Beijing, China) according to each manufacturer's protocol. The histological images were obtained using a Zeiss bright field microscope. The histological images were obtained using a Zeiss bright field microscope. Histological scores of the sections were determined blindly by two observers (X.H. and X.T.) based on previously described criteria [29].

2.10.4. Immunohistochemical staining

After dewaxing with xylene, the sections were treated with 3% H_2O_2 in methanol (Sigma-Aldrich) to inhibit endogenous peroxidase activity and 10 mM Tris-EDTA solution (pH 9.0; Sigma-Aldrich) at 65 °C for 1 h. After blocking with a blocking buffer (Beyotime) for 30 min, the sections were incubated with the primary antibody against COL I, COL II, or NRF2 (1:500; Abcam) overnight at 4 °C. The next day, the sections were incubated with a biotinylated secondary antibody (Abcam) for 1 h at room temperature. The sections were stained using an SP immunohistochemistry kit and 3,3′-diamino benzidine solution (DAB; Nanjing Jiancheng Bioengineering Institute, China) to visualize immunoreactivity. The nuclei were counterstained with hematoxylin. The images were captured using a Zeiss bright field microscope. The percentage of positive cells was quantified using the Image J software.

2.11. Statistical analysis

All quantitative values were presented as mean ± standard deviation (x ± s). The Student's t-test was used to compare two groups, whereas the one-way Analysis of Variance (ANOVA) was performed to compare multiple groups. All statistical analyses were performed using PRISM 9 (GraphPad Software, San Diego, CA, USA). *P*-values <0.05 (* or $^{\#}$) or <0.01 (** or $^{\#\#}$) were considered statistically significant.

3. Results

3.1. Melatonin-protected matrix synthesis of AF cells from IL-1β-induced inflammation

We investigated the effect of melatonin on the matrix metabolism of AF cells. Melatonin increased the expression of AF matrix components at both mRNA and protein levels, including COL I, COL II, and aggrecan under normal culture conditions (Suppl. Fig. 1). IL-1β was added into the culture medium to induce an inflammatory environment, resulting in a remarked reduction in the collagen and aggrecan synthesis. In contrast, treatments with melatonin significantly protected the matrix metabolism of AF cells. For instance, treatment with 100 μM melatonin significantly increased the transcript levels of *Col1a1* by 12.5%, *Col2a1* by 9.3%, and *Acan* by 27.0%, compared to the IL-1β-treated cells (Fig. 2A). Western blotting assays revealed that melatonin promoted the protein expression of COL I, COL II, and aggrecan in IL-1β-treated AF cells (Fig. 2B and C). Considering that COL I is the most important component in AF tissues, immunofluorescence staining confirmed that 100 μM melatonin protected the COL I expression from IL-1β stimulation in AF cells (Fig. 2D). These results indicated that melatonin effectively preserved the matrix metabolism of AF cells in an IL-1β-induced inflammatory environment.

3.2. Melatonin rescued the IL-1β-impaired mitochondrial function of AF cells

Mitochondrial function plays an important role in tissue regeneration, providing energy for matrix synthesis and regulating redox homeostasis. We evaluated the protection of melatonin on the mitochondrial function of AF cells in the inflammatory environment. The exposure of AF cells to IL-1β induced an 18.0% reduction in ATP production, whereas melatonin increased it by 12.2% and 20.1% at 1 μM and 100 μM, respectively, compared to the IL-1β group (Fig. 3A). Additionally, melatonin treatments significantly up-regulated the transcript levels of mitochondrial respiratory chain factors. For example, 100 μM melatonin improved the *Sdha* gene expression by 98.3%, *Nd4* by 32.8%, and *Atp5a* by 41.3% in IL-1β-treated cells (Fig. 3B). Consistently, Western blot analyses confirmed that melatonin treatment successfully improved the protein levels of the respiratory chain factors SDHA, ND4, and ATP5A that were impaired by IL-1β stimulation (Fig. 3C and D). Moreover, mitochondrial membrane potentail is critical for the integrity of mitochondria, and immunofluorescence staining suggested that IL-1β treatment significantly decreased the MMP level by 75.4% in AF cells. In contrast, melatonin treatments improved MMP by 28.2% and 39.5% at 1 μM and 100 μM (Fig. 3E and F). These data indicated that melatonin preserved the energy production and mitochondrial function of IL-1β-treated AF cells.

3.3. Melatonin improved intracellular antioxidant functions of AF cells

Since inflammatory cytokines can cause oxidative stress, we investigated whether melatonin mediated antioxidant protection on AF cells. Immunofluorescence experiments examined the intracellular (Fig. 4A) ROS and mitochondrial superoxide levels (Fig. 4B). The exposure of AF cells to IL-1β resulted in dramatic increases in intracellular ROS and mitochondrial superoxide that were 99.1% and 3.2-fold higher than the CTRL group, respectively (Fig. 4C and D). Melatonin treatments dose-dependently attenuated IL-1β-induced oxidative stress. Particularly, 100 μM melatonin reduced the intracellular ROS by 80.2% and mitochondrial superoxide by 66.3% in IL-1β-treated cells. Regarding the antioxidant functions, melatonin treatments effectively improved the intracellular antioxidant enzymes of AF cells at mRNA and protein levels (Suppl. Fig. 2A). After treating with 100 μM melatonin, the SOD2 and HO-1 protein expression was up-regulated by 27.9%, and 34.8%, respectively, compared to the IL-1β group (Fig. 4E and F).

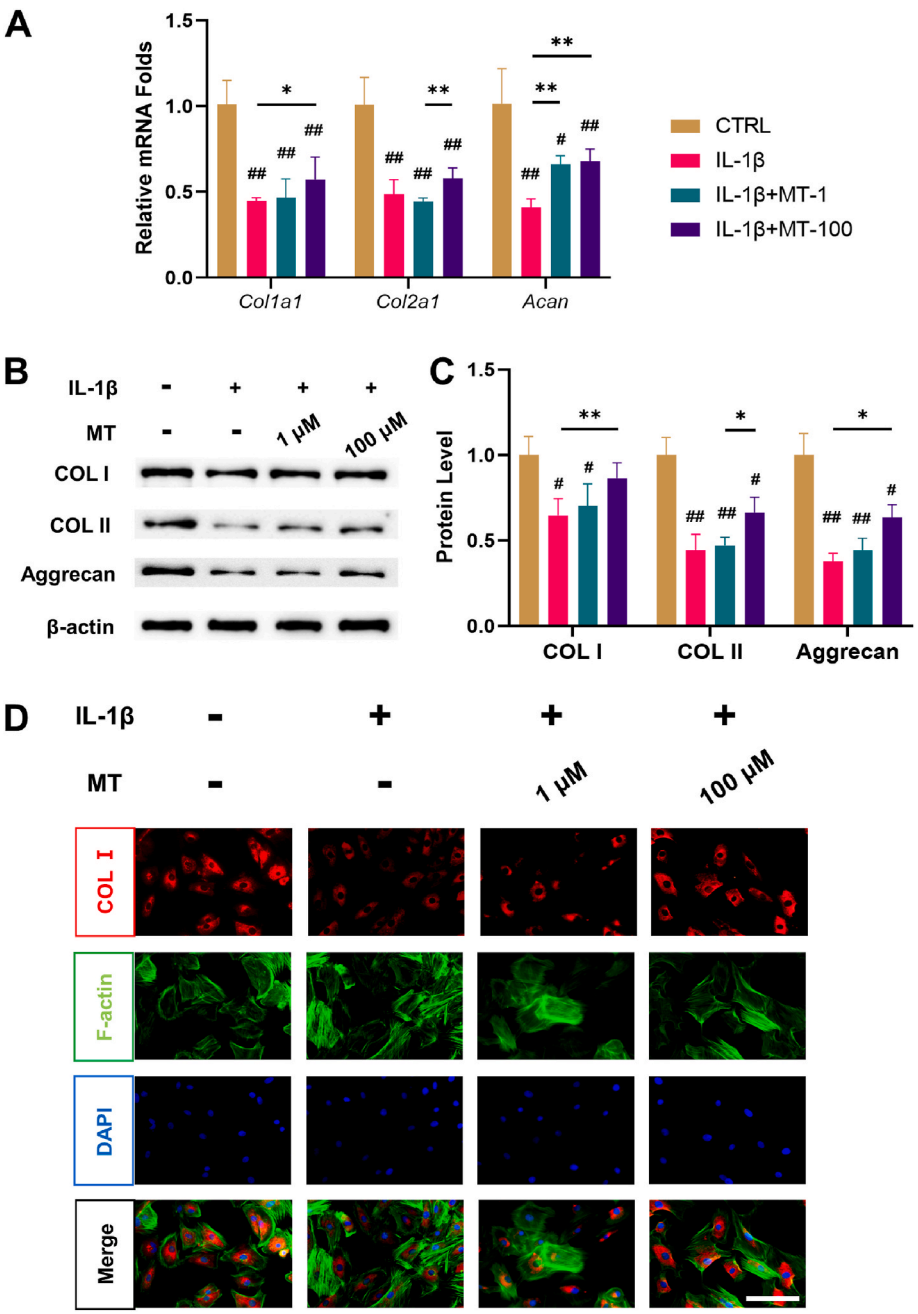

Fig. 2. *In vitro* experiments were conducted to investigate the impact of melatonin on matrix synthesis of AF cells in an inflammatory environment induced by IL-1β. AF cells were exposed to 5 ng/mL IL-1β and treated with melatonin at concentrations of 1 and 100 μM. (A) The gene expressions of *Col1a1*, *Col2a1*, and *Acan* in IL-1β-treated AF cells were evaluated to assess the effect of melatonin, n = 4. (B–C) The protein levels of COL I, COL II, and Aggrecan were determined using Western blot, n = 3. (D) Immunofluorescence staining of COL I was performed to assess the preservation of matrix by melatonin in the presence of IL-1β. Scale bar: 50 μm. Statistically significant differences are indicated by # where $P < 0.05$ or ## where $P < 0.01$ compared to the control (CTRL) group; * where $P < 0.05$ or ** where $P < 0.01$ between the indicated groups.

Immunofluorescence staining confirmed that melatonin-treated cells express SOD2 (Suppl. Fig. 2B). NRF2 is a crucial transcription factor that regulates the antioxidant enzyme expression. We discovered that IL-1β treatment decreased the protein level by 30.2%, whereas 100 μM melatonin increased it by 18.6%. Considering that NRF2 regulates redox homeostasis by binding the antioxidant response element sequence in the nucleus, we performed immunofluorescence staining to investigate the nuclear translocation of NRF2. After melatonin treatments, we observed that the nuclear translocation efficiency was increased by 37.6% and 40.7% at 1 μM and 100 μM, respectively, in IL-1β-stimulated AF cells (Fig. 4G and H). These findings revealed that melatonin treatments alleviated IL-1β-stimulated oxidative stress by activating NRF2 and its downstream intracellular antioxidant enzymes.

3.4. Silencing of *Nrf2* abrogated melatonin-mediated protection on matrix synthesis and energy metabolism of AF cells

AF cells were transfected with siRNA targeting *Nrf2* before melatonin treatment to investigate the role of NRF2 in melatonin-mediated protection of mitochondrial functions. After the transfection, the transcript and protein levels of NRF2 were down-regulated by 79.8% and 51.6%, respectively (Fig. 5A and B). Additionally, HO-1 and SOD2 protein levels

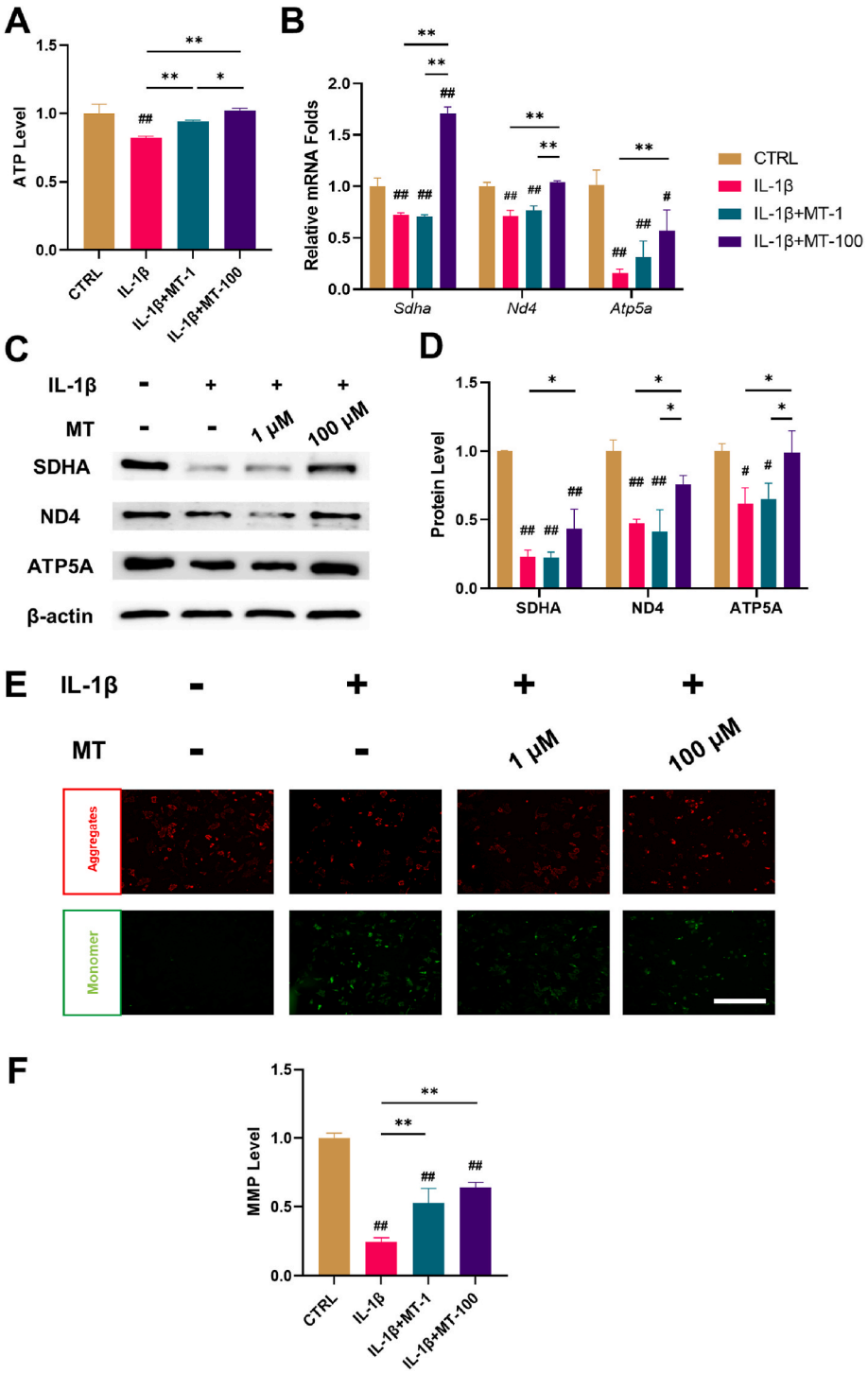

Fig. 3. Melatonin treatments rescued the mitochondrial function of AF cells in the presence of IL-1β. AF cells were exposed to 5 ng/mL IL-1β and treated with melatonin at concentrations of 1 and 100 μM. (A) The effect of melatonin on ATP production of AF cells, n = 4. (B) The gene expressions of mitochondrial respiratory chain factors (*Sdha*, *Nd4*, and *Atp5a)* were quantified with real-time RT-PCR, n = 4. (C–D) The protein levels of SDHA, ND4, and ATP5A were determined using Western blot, n = 3. (E–F) Immunofluorescence staining indicated the effect of melatonin on mitochondrial membrane potential (MMP) levels, n = 3. Scale bar: 200 μm. Statistically significant differences are indicated by # where $P < 0.05$ or ## where $P < 0.01$ compared to the control (CTRL) group; * where $P < 0.05$ or ** where $P < 0.01$ between the indicated groups.

were decreased by 33.5% and 29.1%, respectively, in siRNA-transfected cells (Fig. 5B), consistent with their mRNA expression decreased by 89.3% and 75.8% (Suppl. Fig. 3A). The mitochondrial ROS levels were increased by 2.1-fold by the siRNA transfection (Fig. 5C and D). Moreover, the SDHA, ND4, and ATP5A protein levels were reduced by 24.9%, 36.9%, and 17.6%, respectively, in siRNA-transfected cells (Fig. 5E), consistent with their mRNA expression reduced by 85.8%, 84.5%, and 85.0% (Suppl. Fig. 3B). The ATP content and MMP levels were significantly decreased by 19.5% and 77.2%, respectively, compared to the negative control (NC) group. (Fig. 5F and G). Furthermore, silencing *Nrf2* significantly reduced the matrix synthesis component expression at mRNA and protein levels. The protein levels of COL I, COL II, and

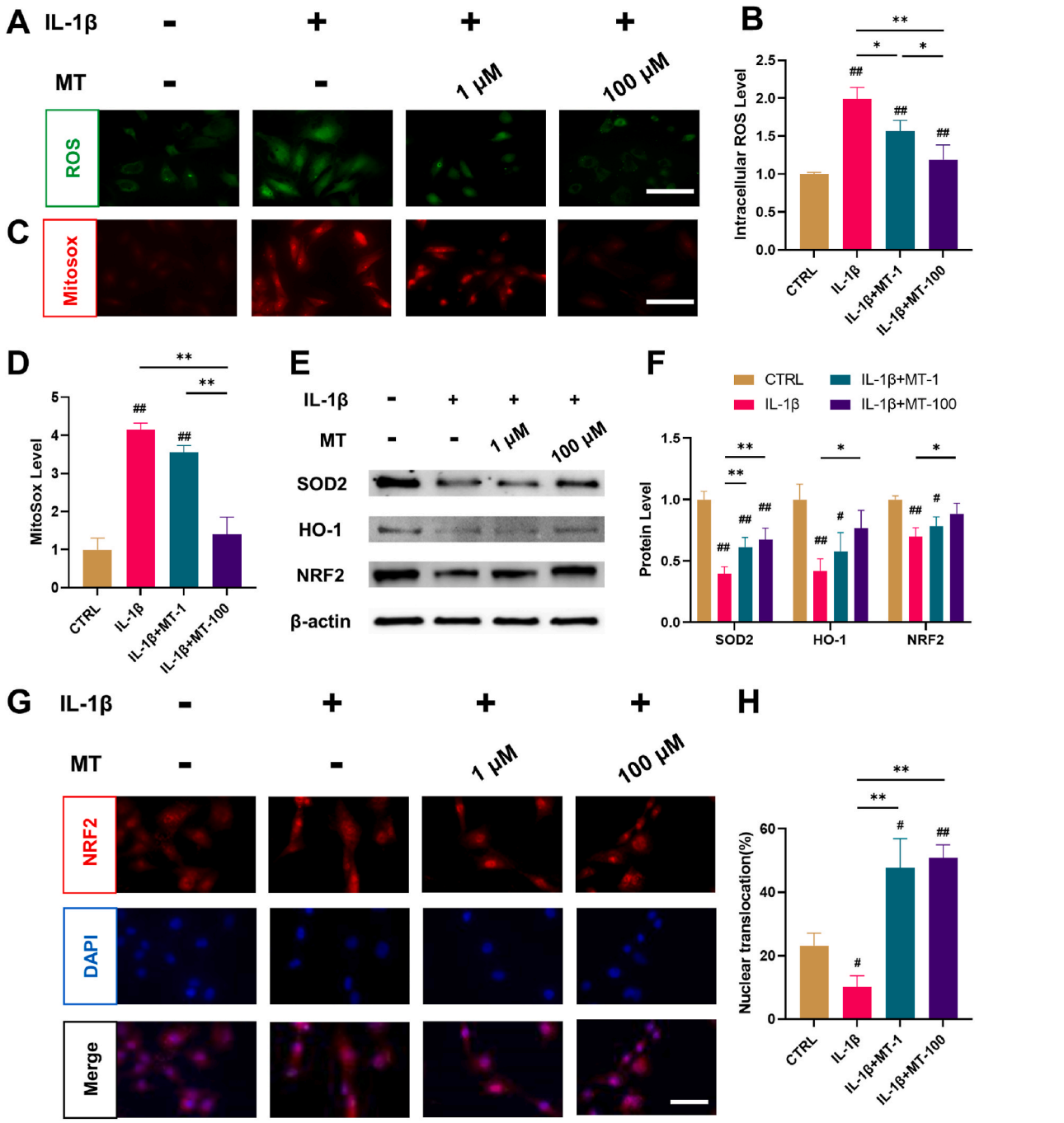

Fig. 4. Melatonin treatments attenuated IL-1β-induced oxidative stress in AF cells through activation of intracellular antioxidant functions. (A–B) Intracellular ROS and mitochondrial superoxide were detected through immunofluorescence staining using DCFH-DA and MitoSOX, respectively. Scale bar: 50 μm. (C–D) Quantification of the levels of intracellular ROS and mitochondrial superoxide, n = 3. (E–F) The protein levels of antioxidant enzyme SOD2 and HO-1 and the transcription factor NRF2 were determined using Western blot, n = 3. (G–H) The efficacy of NRF2 nuclear translocation in AF cells was assessed via immunofluorescence assay, n = 3. Scale bar: 20 μm. Statistically significant differences are indicated by # where $P < 0.05$ or ## where $P < 0.01$ compared to the control (CTRL) group; * where $P < 0.05$ or ** where $P < 0.01$ between the indicated groups.

Aggrecan were significantly decreased by 61.2%, 39.2%, and 57.1%, respectively, in siRNA-transfected cells (Fig. 5H), consistent with their mRNA expression decreased by 73.7%, 95.3%, and 44.9%, respectively (Suppl. Fig. 3C).

3.5. Characterization and biocompatibility of self-healing Hydrogel@MT

The total mercapto content in the Au-Gel-β-CD self-healing hydrogel was 45.3 ± 0.3 μmol/g and the substitution degree was confirmed as 28.20%. Melatonin was incorporated into a Gel-β-CD hydrogel with self-healing properties (Hydrogel@MT) to achieve a sustained release effect. SEM revealed that Hydrogel and Hydrogel@MT had an irregular network structure (Fig. 6A). After the supplementation with gold ions, mercapto-modified gelatin was chemically cross-linked to form a solid hydrogel (Suppl. Fig. 4A). Meanwhile, Hydrogel@MT could be injected with a 22 G needle, indicating that incorporation with melatonin did not affect the injectability of the hydrogel (Suppl. Fig. 4B). A hydrogel was cut and labeled with different colors. The two hydrogels were

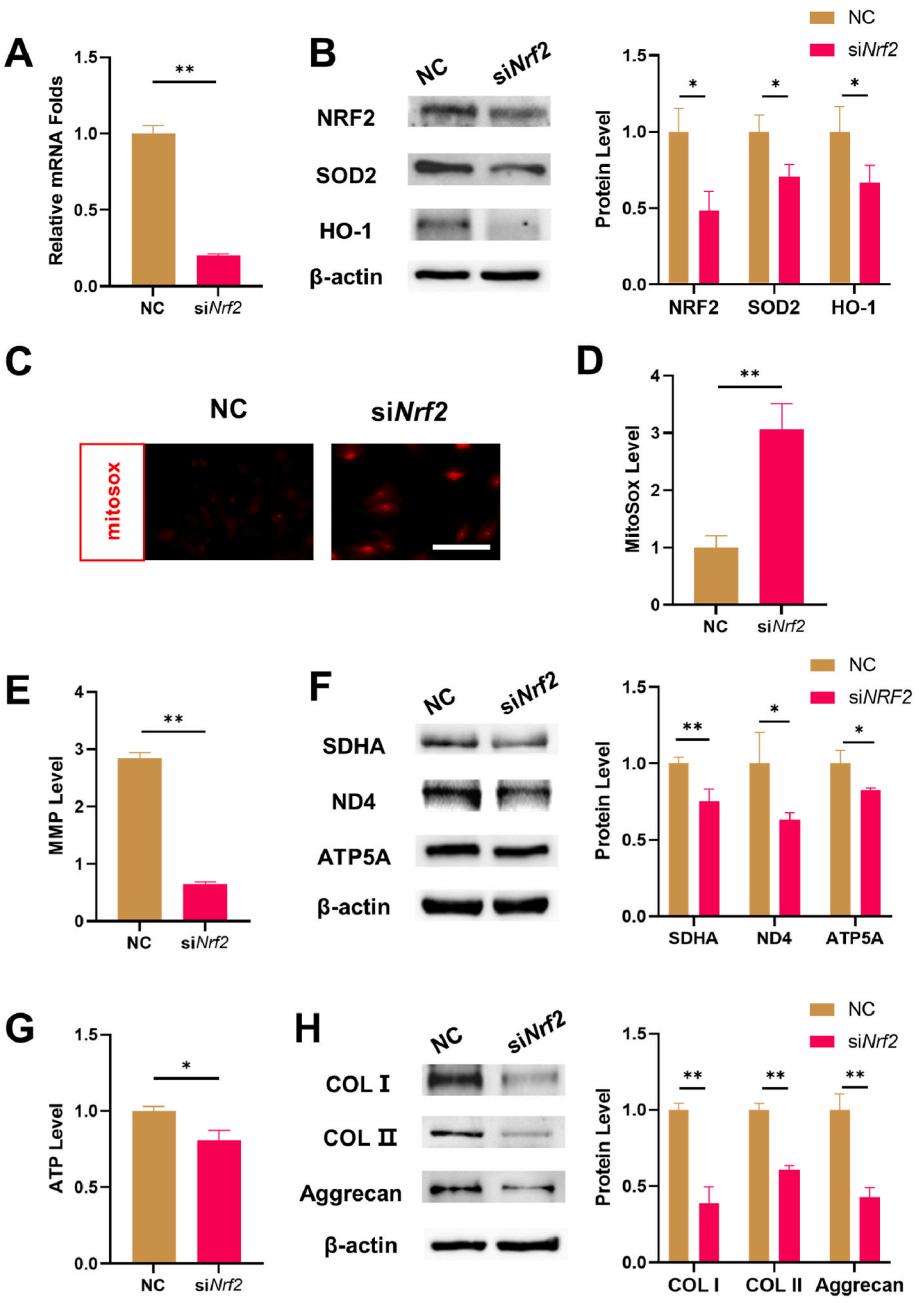

Fig. 5. The protective effect of melatonin on AF cells was abrogated by silencing of *Nrf2* through siRNA. Prior to exposure to 5 ng/mL IL-1β and 100 μM melatonin, AF cells were pre-treated with *Nrf2*-targeting siRNA or negative control (NC) siRNA. (A) The mRNA expression of *Nrf2* was determined by real-time RT-PCR, n = 4. (B) The protein levels of NRF2, SOD2, and HO-1 were measured using Western blot, n = 3. (C–D) Inhibition of *Nrf2* increased the levels of mitochondrial superoxide, n = 3. Scale bar: 50 μm. (E) The MMP levels in siRNA-transfected AF cells, n = 3. (F) The protein levels of mitochondrial respiratory chain factors, including SDHA, ND4, and ATP5A, were determined using Western blot, n = 3. (G) Silencing of *Nrf2* reduced the ATP production in melatonin-treated AF cells, n = 3. (H) The protein levels of COL I, COL II, and Aggrecan were determined using Western blot, n = 3. Statistically significant differences are indicated by * where $P < 0.05$ or ** where $P < 0.01$ between the indicated groups.

reassembled to test the hydrogel self-healing ability. After 1 h, they completely healed without rupture (Suppl. Fig. 4C). The release profile suggested that melatonin could be sustainedly released from the hydrogel for one month, possibly due to cyclodextrin-mediated host-guest chemistry (Fig. 6B). Rheological analysis of hydrogels demonstrated stable values of G′ and G″ at 1 Hz, 37 °C, with G' always being greater than G″, suggesting that hydrogels retained the state of elastic gels (Fig. 6C). Cyclic strain tests indicate that the mechanical properties of hydrogel could recover to the initial after cyclic strain. CCK-8 and Live/dead cell staining exhibited favorable biocompatibility in Hydrogel and Hydogel@MT since the difference was insignificant between the two groups (Suppl. figs. 4D–F). The scratch assay revealed that Hydrogel@MT significantly improved the migration capacity of AF cells by 39.1% (6 h) and 14.8% (12 h) than the hydrogel group (Fig. 6E).

3.6. *In situ implantation of Hydrogel@MT promoted rat AF regeneration*

The box-cut model was created in rat caudal IVDs to investigate the regenerative effect of AF tissues, and self-healing hydrogel loaded with or without MT was implanted into the AF injured site. X-ray and MRI analyses were performed four and eight weeks after implantation (Fig. 7A and B). X-ray imaging revealed that the Defect group yielded the

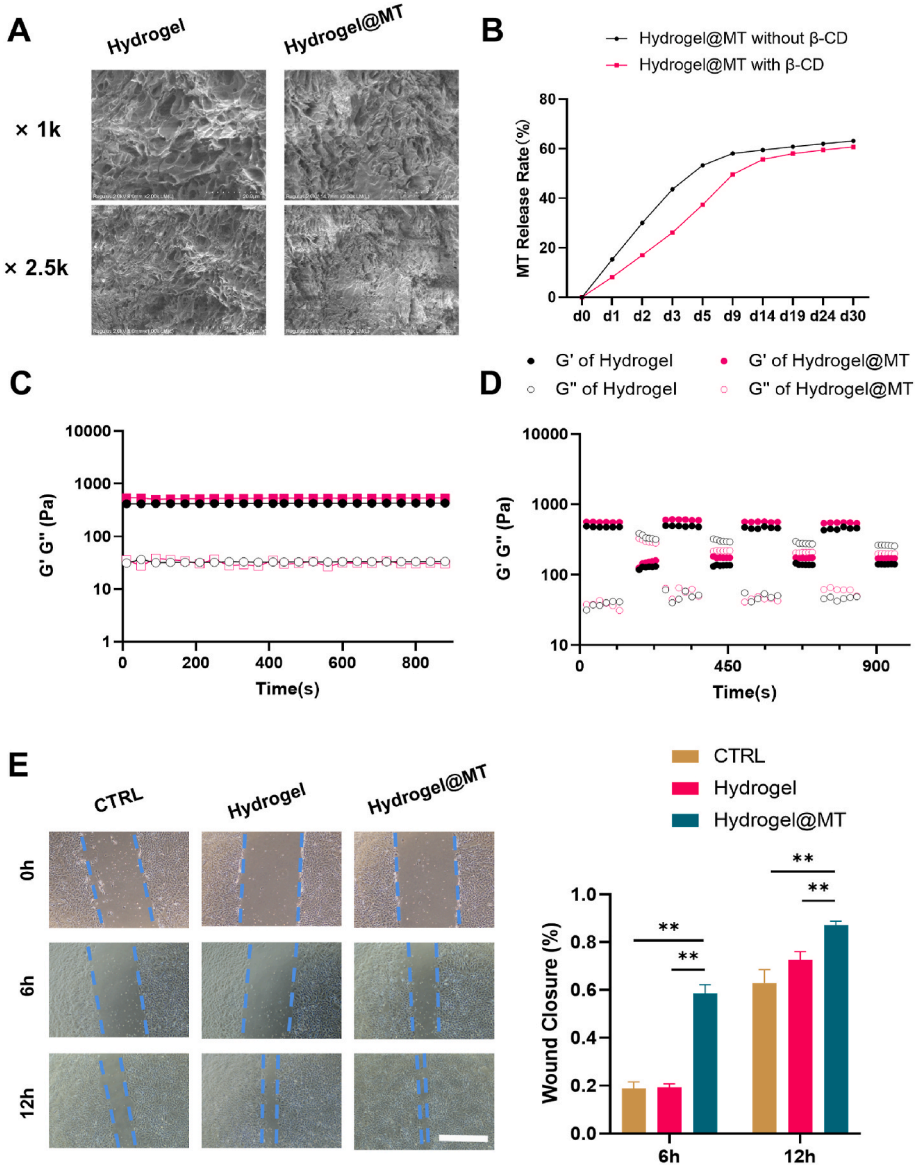

Fig. 6. Characterization of the self-healing hydrogel loaded with melatonin. Melatonin was incorporated into a Gel-β-CD hydrogel (Hydrogel@MT). (A) Representative SEM images of the surface morphology of Hydrogel and Hydrogel@MT. (B) Cumulative release of melatonin from Hydrogel@MT was determined over a period of one month. (C–D) The time sweeps (strain = 1%, frequency = 1 Hz), and the step-strain sweeps (strain = 1 or 300%, frequency = 1 Hz) of the self-healing hydrogels. Temperature at 37 °C. G′, storage modulus; G″, loss modulus. (e) The effect of Hydrogel@MT on the migration ability of AF cells was investigated using scratch assay at 0, 6, and 12 h after treatment with hydrogel leachates, n = 3. Scale bar: 1 mm. Statistically significant differences are indicated by * where $P < 0.05$ or ** where $P < 0.01$ between the indicated groups.

lowest DHI, 72.2% at week four and 66.3% at week eight, compared to the Sham group. Treatment with Hydrogel improved the disc height by 1.3% at week four and 7.0% at week eight compared to the Defect group. Moreover, implantation of Hydrogel@MT effectively restored the disc height, which was 14.0% and 14.8% higher than that of the Defect and Hydrogel groups, respectively, in the eighth week (Fig. 7C). Following the DHI data, the box-cut defect resulted in a significant loss of NP hydration when evaluated quantitatively using MRI. Hydrogel or Hydrogel@MT implants preserved the water content in the NP tissues. The Hydrogel@MT group had the highest level of MRI signals (Fig. 7B). At the eighth week, the MRI signals of the Hydrogel@MT group were 18.4% and 13.0% higher than those of the Defect and Hydrogel groups, respectively (Fig. 7D). These diagnostic imaging results demonstrated that implantation of Hydrogel@MT preserved the disc height and NP hydration in injured IVDs.

The rat caudal IVD samples were harvested after four and eight weeks of the surgery. The gross morphology revealed severe IVD degeneration in the Defect group, whereas Hydrogel@MT preserved the structure of NP and AF tissues (Fig. 8A). H&E staining in the axial plane revealed that the NP was lost, and the box-cut surgery damaged the AF layered structure. Treatment with Hydrogel barely prevented NP loss, indicating that hydrogel alone was ineffective in repairing AF defects or ameliorating IVD degeneration. However, the Hydrogel@MT implant successfully efficiently protected the IVD structure from the box-cut damage, evidenced by the complete structure of the NP and AF tissues, particularly the AF lamellae integrity (Fig. 8B and D). Furthermore, S.O. staining results demonstrated that the Hydrogel@MT implant preserved sulfated glycosaminoglycans (GAGs) deposition in the NP and inside AF tissues (Fig. 8C and E). The Hydrogel@MT group had histological scores of 1.3-fold and 1.2-fold lower than the Defect group at four and eight weeks (Fig. 8F and G).

Immunohistochemical analyses in the axial plane confirmed the loss

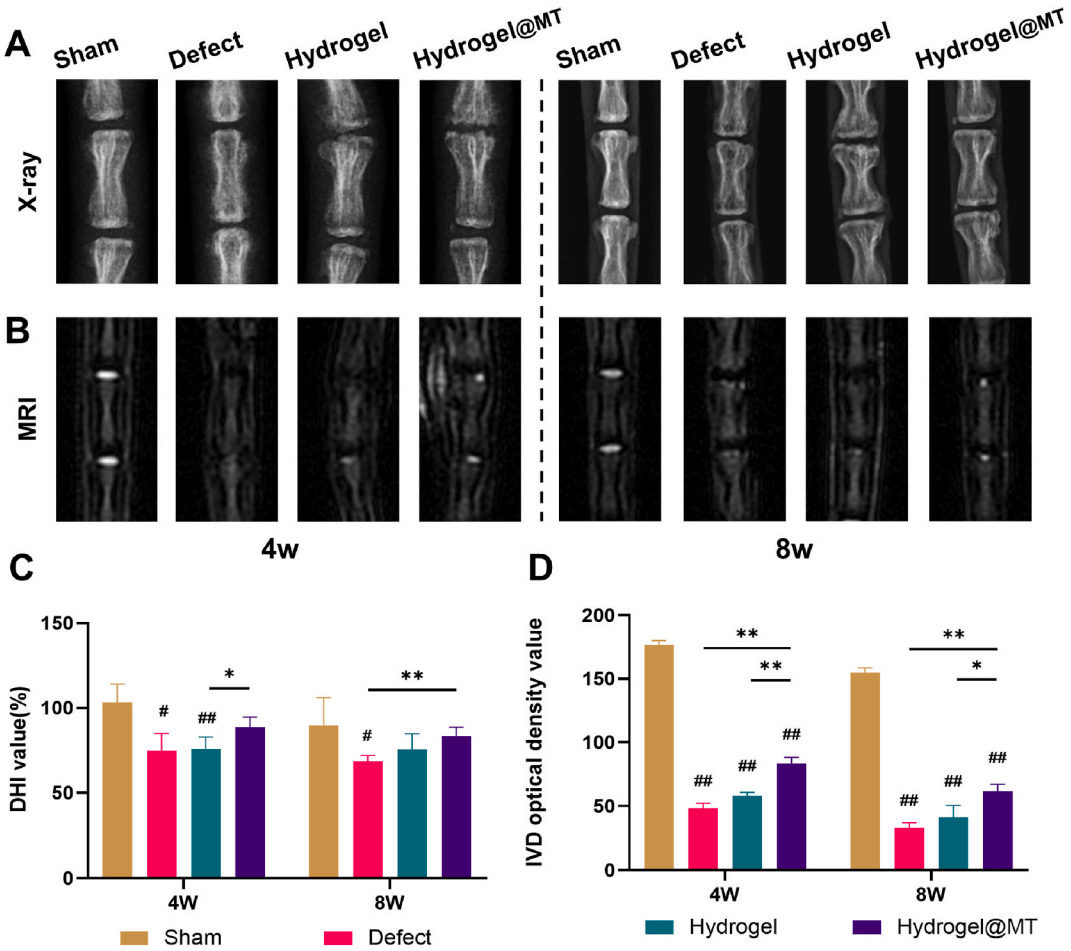

Fig. 7. Diagnostic imaging analyses were conducted to evaluate the impact of Hydrogel@MT on the degeneration of rats' caudal intervertebral discs (IVDs) that were subjected to a box-cut injury. The rats' caudal IVDs were divided into five groups: the Sham group, which served as an intact control, the Defect group, which was induced by a box-cut injury, the Hydrogel group, in which the injured AF was implanted with Hydrogel, and the Hydrogel@MT group, in which the injured AF was implanted with Hydrogel@MT. (A) Representative X-ray images of treated sites in rats' caudal IVDs at 4 and 8 weeks post-surgery. (B) Representative MRI images of treated sites in rats' caudal IVDs 4 and 8 weeks after surgery. (C) The disc height index (DHI) was calculated from the radiograph images, n = 4. (D) The optical density values of IVD based on MRI signals were utilized to indicate the degeneration of rats' caudal IVDs, n = 4. Statistically significant differences are indicated by # where $P < 0.05$ or ## where $P < 0.01$ compared to the Sham group; * where $P < 0.05$ or ** where $P < 0.01$ between the indicated groups.

of collagens I and II in the Defect group, whereas the Hydrogel@MT implant promoted the collagen component deposition in the box-cut injury site after four and eight weeks of the surgery (Fig. 9A and B). Quantitative analysis confirmed that the percentages of collagen I-positive cells in the Hydrogel@MT groups at week eight were 26.1% and 19.9% higher than in the Defect and Hydrogel groups, respectively (Fig. 9C, Suppl. Fig. 5A). Consistently, the percentages of collagen II-positive cells in the Hydrogel@MT group at week eight were increased by 13.8% and 32.5% than the Defect and Hydrogel groups, respectively (Fig. 9D, Suppl. Fig. 5B). Moreover, we observed strong NRF2 expression in the AF defect area of the Hydrogel@MT group than Defect group (Fig. 9A and B). Quantitative analysis confirmed that the proportions of NRF2-positive cells in the Hydrogel@MT group at week eight were 38.2% and 16.9% higher than in the Defect and Hydrogel groups, respectively (Fig. 9E, Suppl. Fig. 5C). The immunohistochemical results demonstrated that Hydrogel@MT implant promoted the AF matrix synthesis in the injury site and protected NP from degeneration by enhancing NRF2 expression.

4. Discussion

The current clinical treatment for IVD herniation is nucleus discectomy; however, if left unrepaired, the lesions in the AF lead to IVD degeneration, including NP tissue dehydration and disc height loss, and eventually compromise the biomechanical properties of IVDs [30]. A strategy for using a self-healing hydrogel based on gold-thiolate/disulfide (Au–S/SS) exchange as an injectable NP replacement material was developed to withstand cyclic high-frequency loading. Nevertheless, it failed to restore NP functions due to irreversible damage after injection [31]. Therefore, incorporating hydrogels and bioactive molecules is necessary for AF repair and regeneration. Here, we demonstrated for the first time that a self-healing and dynamic covalent hydrogel containing cyclodextrin and melatonin facilitated AF regeneration, supporting cell viability in an inflammatory environment and enhancing mitochondrial function to boost the AF matrix synthesis. Moreover, Hydrogel@MT successfully sealed the AF defects in rat caudal IVDs to avoid NP leakage, subsequently preventing IVD degeneration by reducing the herniation risk.

Matrix synthesis capacity is a high priority for AF reconstruction, especially in the presence of inflammatory factors surrounding the AF defects. We discovered that melatonin benefited matrix anabolism in AF cells under an inflammatory condition. The up-regulation of collagen I, II, and aggrecan demonstrated that melatonin effectively protected the matrix synthesis of AF cells from IL-1β stimulation. Zhang et al. reported that melatonin regulated IL-1β-induced remodeling of NP matrix by enhancing aggrecan and type II collagen expression while suppressing

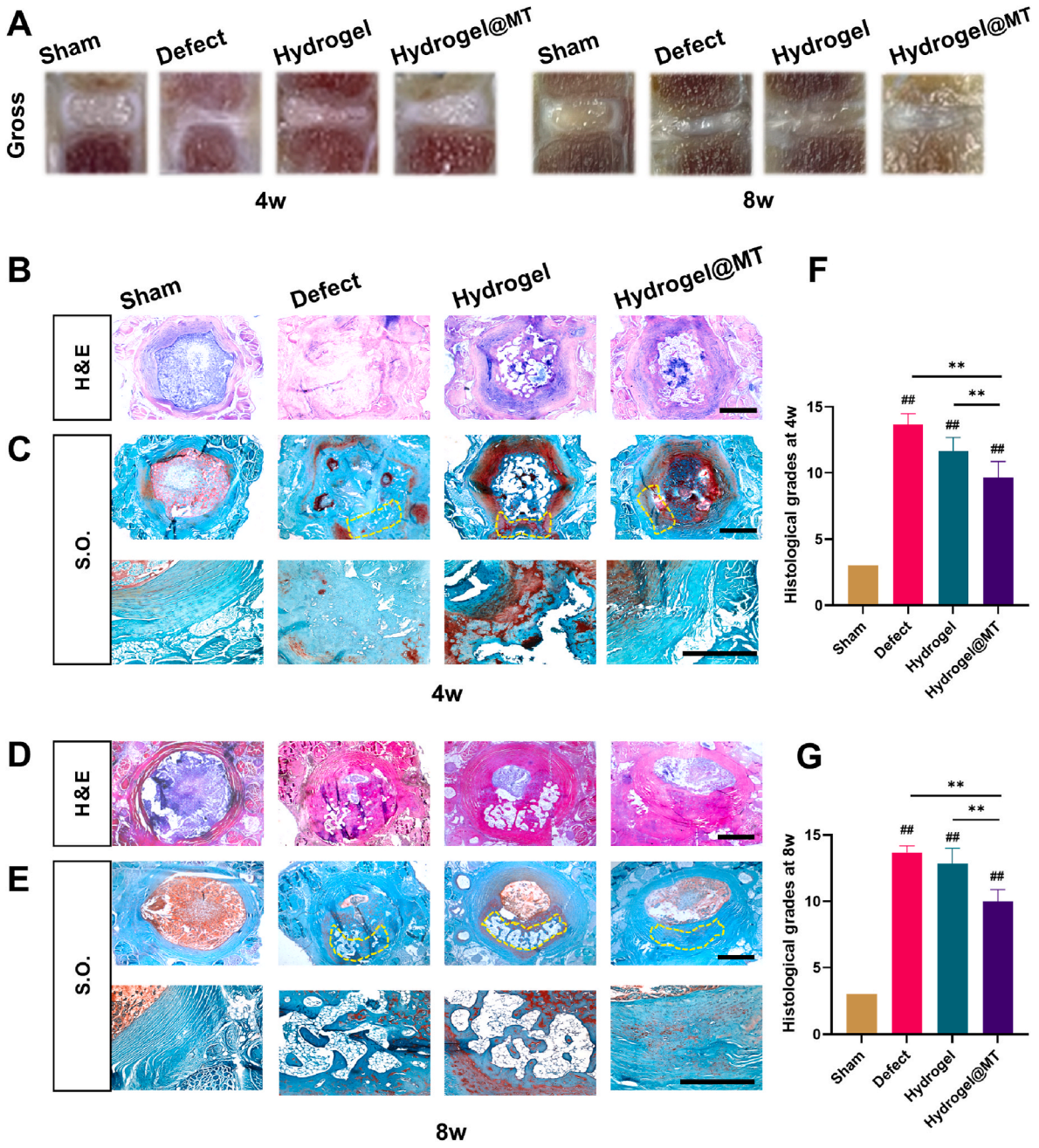

Fig. 8. Histological analysis in the axial plane was conducted to investigate the effect of Hydrogel@MT on annulus fibrosus (AF) regeneration in rats' caudal intervertebral discs (IVDs) with box-cut defects. (A) Gross morphologies of rats' caudal IVDs at 4 and 8 weeks post-surgery. (B–C) Representative images of hematoxylin and eosin (H&E) and Safranin O (S.O.) staining of IVDs at 4 weeks after surgery were obtained, with the AF defect marked by a yellow wireframe. Scale bar: 500 μm. (D–E) Representative images of H&E and S.O. staining of IVDs at 8 weeks after the surgery. Scale bar: 500 μm. (F–G) Histological scores of the untreated and treated IVDs at 4 and 8 weeks post-surgery, n = 4. Statistically significant differences are indicated by # where $P < 0.05$ or ## where $P < 0.01$ compared to the Sham group; * where $P < 0.05$ or ** where $P < 0.01$ between the indicated groups.

matrix degradation enzyme levels, such as matrix metalloproteinase-3 [14]. The inflammatory factor IL-1β reduced AF matrix synthesis capacity via specific signal transduction, specifically the nuclear factor-light-chain-enhancer of activated B cells (NF-κB) pathway [32]. IL-1β stimulation activated the NF–B pathway via NF-κB translocation from the cytoplasm to the nucleus and selective binding to co-activators, such as Creb-binding protein (CPB)/p300. The NF-κB activation inhibits the SOX9 expression, a key transcription factor in chondrogenic differentiation and cartilage matrix production [33]. Gao et al. demonstrated that melatonin attenuated the NF-κB signaling pathway by suppressing the P65 phosphorylation level and rescued the IL-1β-impaired chondrogenic differentiation of human mesenchymal stem cells (MSCs) by preserving the SOX9 expression [34]. Similarly, receptor activator of NF-κB ligand (RANKL) induced osteoclast differentiation, and melatonin demonstrated inhibitory effects on multinucleated osteoclast formation by restraining the nucleus translocation of NF-κB in RANKL-stimulated monocytes [35]. Thus, melatonin's anti-inflammatory effect contributed to the anabolic metabolism of the AF matrix in the presence of IL-1β. In addition, it has been evidenced that the circadian clock plays a role in upholding homeostasis in the IVD and mitigating IVD degeneration caused by abnormal mechanical loading through the down-regulation of the core clock factor brain and muscle Arnt-like protein-1

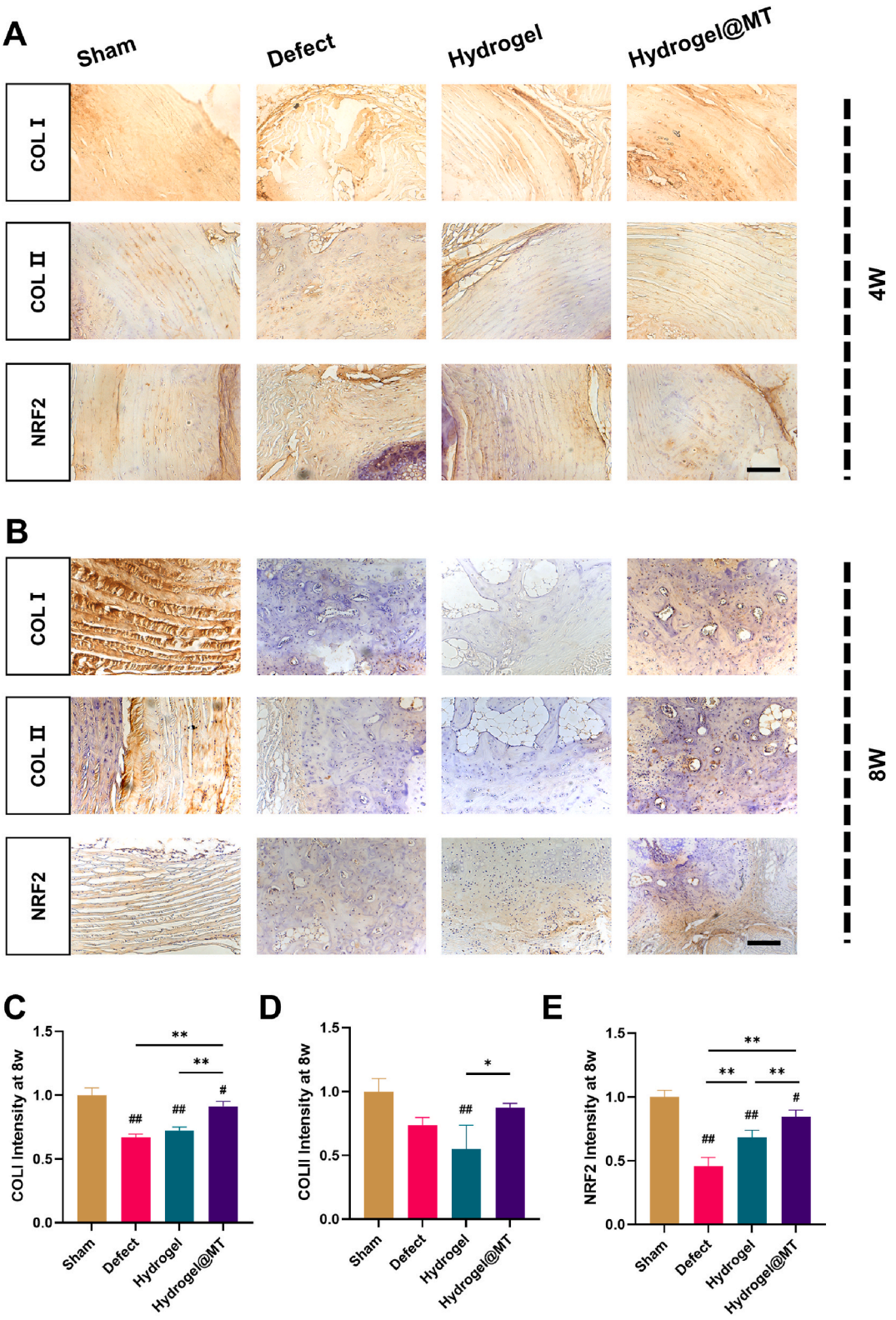

Fig. 9. Immunohistochemical (IHC) analysis in the axial plane was conducted to investigate the annulus fibrosus (AF) regeneration in rats' caudal intervertebral discs (IVDs) with box-cut defects. (A–B) Representative images of IHC staining for collagen I (COL I), collagen II (COL II), and NRF2 in the AF defect site at 4 and 8 weeks post-surgery. Scale bar: 200 μm. (C–E) Quantitative analysis of the percentages of COL I, COL II, and NRF2-positive cells in the AF defect site at 8 weeks post-surgery, n = 4. Statistically significant differences are indicated by # where $P < 0.05$ or ## where $P < 0.01$ compared to the Sham group; * where $P < 0.05$ or ** where $P < 0.01$ between the indicated groups.

(BMAL1). The overexpression of BMAL1 via lentivirus or treatment with melatonin has been found to substantially maintain the integrity of the IVD and effectively shield against matrix degradation induced by compression [36]. Chen and collegeus developed a circadian clock-regulating microsphere by chemically cross-linking polyvinyl alcohol with modified-phenylboronic acid and incorporating melatonin-loaded liposomes. The researchers demonstrated that these melatonin-loaded microspheres effectively enhanced NP tissue regeneration by upregulating the expression of core circadian clock genes through activation of the phosphatidylinositol-3-kinase (PI3K)/protein kinase B (AKT) pathway [37].

Mitochondrial dysfunction has been reported in the pathogenesis of age-related degenerative diseases, such as IVD degeneration and osteoarthritis. Abnormal mechanical loading resulted in aberrant activation of hypoxia-inducible factor (HIF) 1α in EP and AF tissues responsible for enhancing glycolytic metabolism, implying that HIF1α-induced mitochondrial dysfunction caused pathological changes in IVD degeneration [38]. Intra-articular delivery of melatonin recharged the mitochondria of OA chondrocytes by restoring energy metabolism in post-traumatic OA rats, thus representing a promising strategy for protecting cartilage from OA-induced degeneration [17]. Additionally, maintaining mitochondrial function and homeostasis is important for treating IVD degeneration. Cheng et al. developed a partial reprogramming strategy by transiently inducing expression of Oct-3/4, Sox2, Klf4, and c-Myc (OSKM) in NP cells. They demonstrated that short-term induction of OSKM-activated energy switch reduced senescence-related phenotypes in aging NP cells and inhibited the progression of IVD degeneration by up-regulating Hexokinase 2 (HK2) expression to redistribute cytoskeleton [39]. This study demonstrated for the first time that melatonin-laden dynamic hydrogel promoted AF tissue regeneration by improving mitochondrial energy metabolisms, such as ATP production and MMP levels. Functionalizing hydrogel scaffolds with alanyl-glutamine proved effective in promoting rabbit knee articular cartilage repair via regulation of the metabolic microenvironment and attenuation of mitochondrial oxidative stress [40]. Besides the mitochondrial protection effect, melatonin may mediate anti-inflammatory properties by inhibiting the NLR pyrin domain containing 3 (NLRP3) inflammasome activation. Chen et al. demonstrated that IL-1β promoted its expression by up-regulating NLRP3 inflammasome activation during IVD degeneration, and melatonin treatment disrupted the IL-1β/NLRP3 inflammasome activation positive feedback loop [41]. Therefore, future research will illustrate the underlying mechanism of melatonin regulating NLRP3 inflammasome activation in AF defect repair.

The enhancement of mitochondrial energy metabolism causes an increase in ROS production due to the electron leakage from the respiratory chain, requiring the activation of the intracellular antioxidant system to scavenge free radicals. NRF2 can confer adaptive protection against oxidative stress in IVD cells, while deficiency of NRF2 aggravates IVD degeneration by reducing autophagy-related gene expression and inhibiting the subsequent antioxidant feedback loop [42]. Melatonin treatment activates the NRF2 pathway and its downstream antioxidant enzyme heme oxygenase 1 (HO-1) to prevent cartilage degeneration by suppressing matrix degradation enzyme expression in the early stages of osteoarthritis. Melatonin significantly increased the NRF2 protein levels rather than its mRNA expression by inhibiting miR-146a, a predicted target for *Nrf2* post-transcriptional regulation [43]. A ROS scavenging strategy has been developed to improve the bone microenvironment during bone defect repair. Sun et al. fabricated ROS-responsive GelMA hydrogel for controllable release of the antioxidant enzyme catalase. This hydrogel could provide prolonged oxygen supply by degrading hydrogen peroxide and generating oxygen and facilitated bone regeneration in a mice skull defect model by enhancing angiogenesis and osteogenesis [44]. We encapsulated melatonin in cyclodextrin and incorporated it into a seal-healing hydrogel inspired by the microenvironment regulation. Melatonin sustained release eliminated excessive ROS and improved mitochondrial function to meet the matrix anabolism demand in the AF defect region. Therefore, a self-healing hydrogel with energy metabolism regulatory function and NRF2-mediated antioxidant protection has great clinical therapeutic potential.

Recently, there has been significant progress in the development of self-healing hydrogel, which possesses the remarkable capability to autonomously restore its structural integrity following damage. This advancement has led to the exploration of diverse applications, particularly in the field of regenerative medicine. Notably, the implementation of dynamic crosslinking networks has demonstrated substantial potential in the creation of self-healing hydrogel dressing materials. These materials exhibit the ability to mitigate dressing damage resulting from physical activity, thereby presenting a promising solution for joint wound dressings [24]. Furthermore, the utilization of self-healing hydrogels in the treatment of chronic wounds, such as those associated with diabetes, offers the advantage of maintaining structural stability throughout the protracted healing process [45]. Self-healing hydrogels have been developed for use as carriers of drugs or cells, as well as support matrices for targeted injection through minimally invasive surgical procedures, thereby presenting a promising approach in the treatment of brain diseases [46]. Consequently, these findings pertaining to self-healing hydrogels underscore their potential for wider clinical applications.

Surgical discectomy is a current standard procedure for treating IVD herniation. We chose a deeply box-cut defect AF model in the rat caudal IVDs, whose defect thickness was approximately 80% of the whole AF tissue, to mimic the IVD injury in the clinic as closely as possible. Constant et al. compared three different AF defect types in sheep, including slit, cruciate, and box-cut AF defects. They demonstrated that the box-cut AF defect was a suitable IVD injury model that led to histopathologically degenerative and inflammatory changes in IVDs, as evidenced by a significant decrease in NP hydration and the greatest disc height loss among the three models [47]. In this study, we observed inflammation in the AF defect area, a significant reduction of disc height, dehydration of NP tissue, and absence of glycosaminoglycans in the NP area in the defect group after four weeks of surgery, indicating severe IVD degeneration due to the box-cut AF surgery. Nevertheless, melatonin-loaded self-healing hydrogel successfully repaired the AF box-cut defect, but it only partly restored the NP hydration and failed to prevent IVD degeneration completely. Therefore, the integration of NP and AF repair strategies is necessary because the composite composition of the IVD renders individual NP or AF repair therapy for IVD degeneration inadequate. Sloan et al. developed a combined IVD repair strategy based on NP augmentation using hyaluronic acid injection and AF repair using a photo-crosslinked collagen patch. This combined approach effectively healed AF defects, restored NP hydration, and prevented IVD degeneration by preserving the mechanical function of the lumbar spine in a sheep model [48]. Future studies will treat NP and AF as integrity when developing IVD repair and regeneration strategies.

5. Conclusion

We demonstrated that *in vitro* treatment with melatonin protected AF cells from IL-1β-induced inflammatory environment by preserving their matrix synthesis capacity. The protection of melatonin also rescued IL-1β-impaired cellular energy metabolism of AF cells and improved their mitochondrial function, such as MMP and respiratory chain factor expression. The underlying mechanism investigation revealed that the NRF2-mediated antioxidant pathway played a crucial role in regulating mitochondrial redox homeostasis since silencing of *Nrf2* abrogated melatonin's protection on energy metabolism and matrix anabolism of AF cells. Furthermore, a novel melatonin-loaded dynamic hydrogel was developed with favorable biocompatibility and self-healing properties. The self-healing melatonin-loaded hydrogel successfully repaired a box-cut defect in rat caudal AF tissue and prevented subsequent IVD degeneration by preserving NP hydration and matrix metabolism. Melatonin-mediated enhancement of mitochondrial energy metabolism

represents a promising strategy for AF regeneration and treatment of IVD degeneration. Future studies will focus on a combination of NP and AF repair strategies to restore the biomechanical and physiological functions of lumbar IVDs.

CRediT authorship contribution statement

Xiayu Hu: Data curation, Formal analysis, Writing – original draft. Xin Tian: Data curation, Formal analysis, Writing – review & editing. Chunju Yang: Data curation, Formal analysis, Writing – review & editing. Feng Ling: Data curation, Writing – review & editing. Hao Liu: Data curation, Writing – review & editing. Xuesong Zhu: Methodology, Writing – review & editing. Ming Pei: Methodology, Writing – review & editing. Huiling Yang: Methodology, Writing – review & editing. Tao Liu: Formal analysis, Funding acquisition, Investigation, Writing – original draft, Writing – review & editing. Yong Xu: Formal analysis, Funding acquisition, Investigation, Writing – original draft, Writing – review & editing. Fan He: Conceptualization, Project administration, Supervision, Formal analysis, Funding acquisition, Writing – original draft, Writing – review & editing.

Declaration of Competing interest

The authors declare that they have no known competing financial interests or personal relationships that could have appeared to influence the work reported in this paper.

Data availability

Data will be made available on request.

Acknowledgement

This study was supported by the Natural Science Foundation of Jiangsu Province (BK20220046, SBK2023043711); the National Natural Science Foundation of China (82072476, 82302664); Key Laboratory of Orthopaedics of Suzhou (SZS2022017); the Priority Academic Program Development of Jiangsu Higher Education Institutions (PAPD). We want to thanks for Home for Researchers editorial team (www.home-for-researchers.com) for their language editing services.

Appendix A. Supplementary data

Supplementary data to this article can be found online at https://doi.org/10.1016/j.mtbio.2023.100811.

References

[1] N.N. Knezevic, K.D. Candido, J.W.S. Vlaeyen, J. Van Zundert, S.P. Cohen, Low back pain, Lancet 398 (2021), 10294.
[2] N. Fine, S. Lively, C.A. Séguin, A.V. Perruccio, M. Kapoor, R. Rampersaud, Intervertebral disc degeneration and osteoarthritis: a common molecular disease spectrum, Nat. Rev. Rheumatol. 19 (3) (2023) 136–152.
[3] N. Newell, J.P. Little, A. Christou, M.A. Adams, C.J. Adam, S.D. Masouros, Biomechanics of the human intervertebral disc: a review of testing techniques and results, J. Mech. Behav. Biomed. Mater. 69 (2017) 420–434.
[4] P.P. Vergroesen, I. Kingma, K.S. Emanuel, R.J. Hoogendoorn, T.J. Welting, B.J. van Royen, J.H. van Dieën, T.H. Smit, Mechanics and biology in intervertebral disc degeneration: a vicious circle, Osteoarthritis Cartilage 23 (7) (2015) 1057–1070.
[5] Y. Li, L. Chen, Y. Gao, X. Zou, F. Wei, Oxidative stress and intervertebral disc degeneration: pathophysiology, signaling pathway, and therapy, Oxid. Med. Cell. Longev. 2022 (2022), 1984742.
[6] J.A. Bolduc, J.A. Collins, R.F. Loeser, Reactive oxygen species, aging and articular cartilage homeostasis, Free Radic. Biol. Med. 132 (2019) 73–82.
[7] Y. Hu, Z. Shao, X. Cai, Y. Liu, M. Shen, Y. Yao, T. Yuan, W. Wang, F. Ding, L. Xiong, Mitochondrial pathway is involved in advanced glycation end products-induced apoptosis of rabbit annulus fibrosus cells, Spine 44 (10) (2019) E585–E595.
[8] A. Dimozi, E. Mavrogonatou, A. Sklirou, D. Kletsas, Oxidative stress inhibits the proliferation, induces premature senescence and promotes a catabolic phenotype in human nucleus pulposus intervertebral disc cells, Eur. Cell. Mater. 30 (2015) 89–102.
[9] Z. Lin, H. Wang, J. Song, G. Xu, F. Lu, X. Ma, X. Xia, J. Jiang, F. Zou, The role of mitochondrial fission in intervertebral disc degeneration, Osteoarthritis Cartilage 31 (2) (2023) 158–166.
[10] R. Hartman, P. Patil, R. Tisherman, C. St Croix, L.J. Niedernhofer, P.D. Robbins, F. Ambrosio, B. Van Houten, G. Sowa, N. Vo, Age-dependent changes in intervertebral disc cell mitochondria and bioenergetics, Eur. Cell. Mater. 36 (2018) 171–183.
[11] Y. Zhang, T. Liu, H. Yang, F. He, X. Zhu, Melatonin: a novel candidate for the treatment of osteoarthritis, Ageing Res. Rev. 78 (2022), 101635.
[12] Z. Cheng, Q. Xiang, J. Wang, Y. Zhang, The potential role of melatonin in retarding intervertebral disc ageing and degeneration: a systematic review, Ageing Res. Rev. 70 (2021), 101394.
[13] J. Ge, Q. Zhou, J. Niu, Y. Wang, Q. Yan, C. Wu, J. Qian, H. Yang, J. Zou, Melatonin protects intervertebral disc from degeneration by improving cell survival and function via activation of the ERK1/2 signaling pathway, Oxid. Med. Cell. Longev. (2019), 5120275, 2019.
[14] Y. Zhang, F. He, Z. Chen, Q. Su, M. Yan, Q. Zhang, J. Tan, L. Qian, Y. Han, Melatonin modulates IL-1β-induced extracellular matrix remodeling in human nucleus pulposus cells and attenuates rat intervertebral disc degeneration and inflammation, Aging 11 (22) (2019) 10499–10512.
[15] Z. Zhang, J. Lin, N. Tian, Y. Wu, Y. Zhou, C. Wang, Q. Wang, H. Jin, T. Chen, M. Nisar, G. Zheng, T. Xu, W. Gao, X. Zhang, X. Wang, Melatonin protects vertebral endplate chondrocytes against apoptosis and calcification via the Sirt1-autophagy pathway, J. Cell Mol. Med. 23 (1) (2019) 177–193.
[16] Y. Chen, Y. Wu, H. Shi, J. Wang, Z. Zheng, J. Chen, X. Chen, Z. Zhang, D. Xu, X. Wang, J. Xiao, Melatonin ameliorates intervertebral disc degeneration via the potential mechanisms of mitophagy induction and apoptosis inhibition, J. Cell Mol. Med. 23 (3) (2019) 2136–2148.
[17] Y. Zhang, M. Hou, Y. Liu, T. Liu, X. Chen, Q. Shi, D. Geng, H. Yang, F. He, X. Zhu, Recharge of chondrocyte mitochondria by sustained release of melatonin protects cartilage matrix homeostasis in osteoarthritis, J. Pineal Res. 73 (2) (2022), e12815.
[18] R.D. Bowles, L.A. Setton, Biomaterials for intervertebral disc regeneration and repair, Biomaterials 129 (2017) 54–67.
[19] Y. Gan, P. Li, L. Wang, X. Mo, L. Song, Y. Xu, C. Zhao, B. Ouyang, B. Tu, L. Luo, L. Zhu, S. Dong, F. Li, Q. Zhou, An interpenetrating network-strengthened and toughened hydrogel that supports cell-based nucleus pulposus regeneration, Biomaterials 136 (2017) 12–28.
[20] T.J. DiStefano, J.O. Shmukler, G. Danias, T. Di Pauli von Treuheim, W.W. Hom, D. A. Goldberg, D.M. Laudier, P.R. Nasser, A.C. Hecht, S.B. Nicoll, J.C. Iatridis, Development of a two-part biomaterial adhesive strategy for annulus fibrosus repair and ex vivo evaluation of implant herniation risk, Biomaterials 258 (2020), 120309.
[21] L. Yang, C. Yu, X. Fan, T. Zeng, W. Yang, J. Xia, J. Wang, L. Yao, C. Hu, Y. Jin, Y. Zhu, J. Chen, Z. Hu, Dual-dynamic-bond cross-linked injectable hydrogel of multifunction for intervertebral disc degeneration therapy, J. nanobiotechnology 20 (1) (2022) 433.
[22] D.L. Taylor, M. In, Het panhuis, self-healing hydrogels, Adv Mater 28 (41) (2016) 9060–9093.
[23] Y. Tu, N. Chen, C. Li, H. Liu, R. Zhu, S. Chen, Q. Xiao, J. Liu, S. Ramakrishna, L. He, Advances in injectable self-healing biomedical hydrogels, Acta Biomater. 90 (2019) 1–20.
[24] A. Zhang, Y. Liu, D. Qin, M. Sun, T. Wang, X. Chen, Research status of self-healing hydrogel for wound management: a review, Int. J. Biol. Macromol. 164 (2020) 2108–2123.
[25] A. Zhang, Z. Cheng, Y. Chen, P. Shi, W. Gan, Y. Zhang, Emerging tissue engineering strategies for annulus fibrosus therapy, Acta Biomater. 167 (2023) 1–15.
[26] Y. Zhang, W. Yin, Y. Liu, M. Hou, Q. Shi, T. Liu, M. Wang, H. Yang, G. Pan, F. He, X. Zhu, Dynamic protein hydrogel with supramolecularly enveloped kartogenin promotes cartilage regeneration through mitochondrial activation, Compos. B Eng. 246 (2022), 110257.
[27] F. Han, Q. Yu, G. Chu, J. Li, Z. Zhu, Z. Tu, C. Liu, W. Zhang, R. Zhao, H. Mao, F. Han, B. Li, Multifunctional nanofibrous scaffolds with angle-ply microstructure and Co-delivery capacity promote partial repair and total replacement of intervertebral disc, Adv. Healthc. Mater. 11 (19) (2022), e2200895.
[28] K. Vincent, S. Mohanty, R. Pinelli, R. Bonavita, P. Pricop, T.J. Albert, C.L. Dahia, Aging of mouse intervertebral disc and association with back pain, Bone 123 (2019) 246–259.
[29] K. Masuda, Y. Aota, C. Muehleman, Y. Imai, M. Okuma, E.J. Thonar, G. B. Andersson, H.S. An, A novel rabbit model of mild, reproducible disc degeneration by an anulus needle puncture: correlation between the degree of disc injury and radiological and histological appearances of disc degeneration, Spine 30 (1) (2005) 5–14.
[30] Y. Purushothaman, N. Yoganandan, D. Jebaseelan, H. Choi, J. Baisden, External and internal responses of cervical disc arthroplasty and anterior cervical discectomy and fusion: a finite element modeling study, J. Mech. Behav. Biomed. Mater. 106 (2020), 103735.
[31] A. Pérez-San Vicente, M. Peroglio, M. Ernst, P. Casuso, I. Loinaz, H.J. Grande, M. Alini, D. Eglin, D. Dupin, Self-healing dynamic hydrogel as injectable shock-absorbing artificial nucleus pulposus, Biomacromolecules 18 (8) (2017) 2360–2370.
[32] R. Tisherman, P. Coelho, D. Phillibert, D. Wang, Q. Dong, N. Vo, J. Kang, G. Sowa, NF-κB signaling pathway in controlling intervertebral disk cell response to inflammatory and mechanical stressors, Phys. Ther. 96 (5) (2016) 704–711.
[33] Y. Wei, W. Zhi-Hong, Q. Gui-Xing, Y. Bin, C. Jun, W. Yi-Peng, Extracellular signal-regulated kinase inhibition modulates rat annulus fibrosus cell response to interleukin-1, Spine 38 (17) (2013) E1075–E1081.

[34] B. Gao, W. Gao, Z. Wu, T. Zhou, X. Qiu, X. Wang, C. Lian, Y. Peng, A. Liang, J. Qiu, Y. Zhu, C. Xu, Y. Li, P. Su, D. Huang, Melatonin rescued interleukin 1β-impaired chondrogenesis of human mesenchymal stem cells, Stem Cell Res. Ther. 9 (1) (2018) 162.
[35] L. Zhou, X. Chen, J. Yan, M. Li, T. Liu, C. Zhu, G. Pan, Q. Guo, H. Yang, M. Pei, F. He, Melatonin at pharmacological concentrations suppresses osteoclastogenesis via the attenuation of intracellular ROS, Osteoporos. Int. 28 (12) (2017) 3325–3337.
[36] D. Wang, P. Peng, M. Dudek, X. Hu, X. Xu, Q. Shang, D. Wang, H. Jia, H. Wang, B. Gao, C. Zheng, J. Mao, C. Gao, X. He, P. Cheng, H. Wang, J. Zheng, J.A. Hoyland, Q.J. Meng, Z. Luo, L. Yang, Restoring the dampened expression of the core clock molecule BMAL1 protects against compression-induced intervertebral disc degeneration, Bone Res 10 (1) (2022) 20.
[37] W. Chen, D. Zheng, H. Chen, T. Ye, Z. Liu, J. Qi, H. Shen, H. Ruan, W. Cui, L. Deng, Circadian clock regulation via biomaterials for nucleus pulposus, Adv Mater 35 (32) (2023), e2301037.
[38] Z. Wang, H. Chen, Q. Tan, J. Huang, S. Zhou, F. Luo, D. Zhang, J. Yang, C. Li, B. Chen, X. Sun, L. Kuang, W. Jiang, Z. Ni, Q. Wang, S. Chen, X. Du, D. Chen, C. Deng, L. Yin, L. Chen, Y. Xie, Inhibition of aberrant Hif1α activation delays intervertebral disc degeneration in adult mice, Bone Res 10 (1) (2022) 2.
[39] F. Cheng, C. Wang, Y. Ji, B. Yang, J. Shu, K. Shi, L. Wang, S. Wang, Y. Zhang, X. Huang, X. Zhou, K. Xia, C. Liang, Q. Chen, F. Li, Partial reprogramming strategy for intervertebral disc rejuvenation by activating energy switch, Aging Cell 21 (4) (2022), e13577.
[40] R. Yang, X. Zhang, J. Liu, X. Li, D. Zhou, S. Luan, Functional gelatin hydrogel scaffold with degraded-release of glutamine to enhance cellular energy metabolism for cartilage repair, Int. J. Biol. Macromol. 221 (2022) 923–933.
[41] F. Chen, G. Jiang, H. Liu, Z. Li, Y. Pei, H. Wang, H. Pan, H. Cui, J. Long, J. Wang, Z. Zheng, Melatonin alleviates intervertebral disc degeneration by disrupting the IL-1β/NF-κB-NLRP3 inflammasome positive feedback loop, Bone Res 8 (2020) 10.
[42] Z. Tang, B. Hu, F. Zang, J. Wang, X. Zhang, H. Chen, Nrf2 drives oxidative stress-induced autophagy in nucleus pulposus cells via a Keap1/Nrf2/p62 feedback loop to protect intervertebral disc from degeneration, Cell Death Dis. 10 (7) (2019) 510.
[43] X. Zhou, Y. Zhang, M. Hou, H. Liu, H. Yang, X. Chen, T. Liu, F. He, X. Zhu, Melatonin prevents cartilage degradation in early-stage osteoarthritis through activation of miR-146a/NRF2/HO-1 Axis, J. Bone Miner. Res. 37 (5) (2022) 1056–1072.
[44] H. Sun, J. Xu, Y. Wang, S. Shen, X. Xu, L. Zhang, Q. Jiang, Bone microenvironment regulative hydrogels with ROS scavenging and prolonged oxygen-generating for enhancing bone repair, Bioact. Mater. 24 (2023) 477–496.
[45] G. Chang, Q. Dang, C. Liu, X. Wang, H. Song, H. Gao, H. Sun, B. Zhang, D. Cha, Carboxymethyl chitosan and carboxymethyl cellulose based self-healing hydrogel for accelerating diabetic wound healing, Carbohydr. Polym. 292 (2022), 119687.
[46] J. Xu, S.H. Hsu, Self-healing hydrogel as an injectable implant: translation in brain diseases, J. Biomed. Sci. 30 (1) (2023) 43.
[47] C. Constant, W.W. Hom, D. Nehrbass, E.N. Carmel, C.E. Albers, M.C. Deml, D. Gehweiler, Y. Lee, A. Hecht, S. Grad, J.C. Iatridis, S. Zeiter, Comparison and optimization of sheep in vivo intervertebral disc injury model, JOR spine 5 (2) (2022) e1198.
[48] S.R. Sloan Jr., C. Wipplinger, S. Kirnaz, R. Navarro-Ramirez, F. Schmidt, D. McCloskey, T. Pannellini, A. Schiavinato, R. Härtl, L.J. Bonassar, Combined nucleus pulposus augmentation and annulus fibrosus repair prevents acute intervertebral disc degeneration after discectomy, Sci. Transl. Med. 12 (534) (2020), eaay2380.